

AUTHOR QUERY FORM

	<p>Journal: J. Appl. Phys. Article Number: JAP24-AR-00699</p>	<p>Please provide your responses and any corrections by annotating this PDF and uploading it to AIP's eProof website as detailed in the Welcome email.</p>
---	---	--

Dear Author,

Below are the queries associated with your article; please answer all of these queries before sending the proof back to AIP.

Article checklist: In order to ensure greater accuracy, please check the following and make all necessary corrections before returning your proof.

1. Is the title of your article accurate and spelled correctly?
2. Please check affiliations including spelling, completeness, and correct linking to authors.
3. Did you remember to include acknowledgment of funding, if required, and is it accurate?

Please resize all figures to be single column width (half of page width); and make sure all figures and tables are inserted after the text referencing them

Location in article	Query / Remark: click on the Q link to navigate to the appropriate spot in the proof. There, insert your comments as a PDF annotation.
Q1	Please check that the author name is in the proper order and spelled correctly. Also, please ensure that the author's given and surnames have been correctly identified (given name is highlighted in red and surname appears in blue).
Q2	In the sentence beginning "As described in...", please confirm that "previous section" refers to Sec. IV D.
Q3	AIP does not allow footnotes in the text. Please check the incorporation of FN into the text.
Q4	In the sentence beginning "Although predicting the...", please confirm that "next section" refers to Sec. VI.
Q5	Please provide complete details in Refs. 1, 2, 34, 37, and 38.
Q6	Please supply journal title and page number in Ref. 5.
Q7	Please provide volume number in Refs. 5 and 50.
Q8	Please supply publisher's name for Ref. 9.
Q9	We were unable to locate a digital object identifier (doi) for Refs. 27, 40, and 49. Please verify and correct author names and journal details (journal title, volume number, page number, and year) as needed and provide the doi. If a doi is not available, no other information is needed from you. For additional information on doi's, please select this link: http://www.doi.org/ .
Q10	The resolution of Figs. 2 to 14 is low. If you are not satisfied with the way the figures appear in the proof, please provide new figure files of higher resolution.

Please confirm ORCIDs are accurate. If you wish to add an ORCID for any author that does not have one, you may do so now. For more information on ORCID, see <https://orcid.org/>.

[Ellen Wang](#)-0009-0004-0482-5402

Please check and confirm the Funder(s) and Grant Reference Number(s) provided with your submission:

Please add any additional funding sources not stated above:

Thank you for your assistance.

1 A study on Arctic sea ice dynamics using the continuous spin Ising model

2
 3 Cite as: J. Appl. Phys. **135**, 000000 (2024); doi: [10.1063/5.0202612](https://doi.org/10.1063/5.0202612)
 4 Submitted: 5 February 2024 · Accepted: 29 April 2024 ·
 Published Online: ■■■ 2024



5
 6 Ellen Wang^a

7 AFFILIATIONS

Q1 8 Horace Mann School, Bronx, New York, USA

9
 10 ^aAuthor to whom correspondence should be addressed: ellen.ls.wang@gmail.com

12 ABSTRACT

13 The Ising model, initially proposed about 100 years ago to explain ferromagnetism and phase transitions, has become a central pillar of statis-
 14 tical physics and a powerful tool for diverse applications in other fields including environmental studies. In this paper, we introduce con-
 15 tinuous spin values between -1 and $+1$ to a two-dimensional Ising model and utilize the generalized Ising lattice to simulate the dynamics
 16 of sea ice/water transition for a large area of $1500 \text{ km} \times 1500 \text{ km}$ in the Arctic region. The simulation process follows the Metropolis-
 17 Hastings algorithm and incorporates an innovative factor to account for the inertia of spin value changes. Using the sea ice concentration
 18 data collected by the National Snow and Ice Data Center, our results exhibit striking similarity between the simulated and the observed ice
 19 melting and freezing dynamics, and two numerical measures from the simulation—the ice coverage percentage and the ice extent—match
 20 closely with the data statistics. Moreover, the model's best-fit parameters demonstrate the substantial impact of the external forces, which
 21 can be further enriched and linked to the environmental factors in other climate change research.

22 © 2024 Author(s). All article content, except where otherwise noted, is licensed under a Creative Commons Attribution (CC BY) license
 (<https://creativecommons.org/licenses/by/4.0/>). <https://doi.org/10.1063/5.0202612>

24 I. INTRODUCTION

25 This study models Arctic Sea Ice dynamics at a large scale by
 26 innovating on the centennial Ising model (IM). The rapid Arctic
 27 sea ice loss observed in recent years^{1,2} and the hottest year 2023
 28 recorded on the earth³ make our study particularly meaningful.
 29 Upon the classical binary-spin Ising^{4,5} setup, we first introduce the
 30 continuous spin values^{6,7} and then enhance the model by incorpo-
 31 rating a novel inertia factor. The simulated evolution of ice/water
 32 phase transition follows the Metropolis-Hastings⁸ Monte Carlo
 33 process governed by this generalized model. The Arctic sea ice
 34 images collected by the National Snow and Ice Data Center⁹ serve
 35 as the inputs into our model, which outputs the best-fit Ising
 36 parameters and the simulated sea ice configurations. Our analyses
 37 of the simulated configurations and the numeric measures calculated
 38 from the simulation results validate the strong explanatory power of
 39 our generalized model in sea ice studies. After a brief review on the
 40 Ising literature and an introduction of the significance of Arctic sea
 41 ice, Sec. II lays out the theoretical framework of our generalized Ising
 42 model, Sec. III describes the Arctic sea ice data, Sec. IV illustrates the
 43 computational setup, and Sec. V presents the results and analysis, fol-
 44 lowed by final discussions in Sec. VI.

A. Ising model

45 The classical Ising model is the backbone of this study. It was
 46 first formalized by physicists Ernst Ising and Wilhelm Lenz to
 47 explain the equilibrium and phase transition in magnetic systems.
 48 The one-dimensional (1D) IM was solved by Ising in his 1924
 49 thesis,^{4,5,10} which proves the non-existence of phase transition in
 50 the 1D IM. In 1944, Lars Onsager¹¹ was able to solve the two-
 51 dimensional (2D) square-lattice IM analytically. Contradictory to
 52 the 1D case, Onsager identified that there exists a critical tempera-
 53 ture $T_c = 2.27 \text{ J}/\text{k}_B$ when the phase transition happens in a 2D IM.
 54 Later studies of IM in higher dimensions have been closely associated
 55 with various developments in advanced 20th-century physics and
 56 mathematical theories, including the transfer-matrix method,^{12,13}
 57 quantum field theory,¹⁴ mean-field theory,¹⁵ etc.⁵⁸

59 Over the years, the IM has found wide success beyond
 60 physics. Specifically, the Kinetic IM,^{15–17} built upon the equilib-
 61 rium version, has been proposed to analyze biology, environmental
 62 science, machine learning,^{18,19} social science, and economic and
 63 financial systems. These applications are widely implemented as a
 64 discrete time Markov chain of the spin lattice, with spin interac-
 65 tions bounded to finite distance. In biology and neuroscience, IM

66 applications include but are not limited to the condensation of
 67 DNA,²⁰ genetics,²¹ neural networks,^{22,23} neuron spike,²⁴ neuron activity
 68 in cell assemblies,²⁵ and ligands to receptors binding in cells.²⁶
 69 In environmental science, the IM has been employed to investigate
 70 land pattern dynamics.^{27,28} Recently, Ma, Sudakov, Strong, and
 71 Golden have successfully used the 2D IM to capture the essential
 72 mechanism of the ice melt ponds equilibrium configuration.²⁹ In
 73 social science, economics, and finance, the IM has been applied to
 74 research in urban segregation,³⁰ crisis study,³¹ stability of money,³²
 75 etc.

76 B. Arctic sea ice

77 The reversible phase transition between water and ice makes
 78 the IM a great tool to study the dynamics of a surface region with
 79 the co-existence of both states. In this paper, we apply a 2D IM
 80 lattice to study the dynamics of Arctic sea ice melting and freezing
 81 cycles, a major climate change indicator that is of significant environ-
 82 mental, economic, and social significance.³³

83 Sea ice is undoubtedly an integral part of the Arctic Ocean
 84 and the earth.³³ In the dark winter months, ice covers almost the
 85 entirety of the Arctic Ocean, and the ice extent—defined as the per-
 86 centage of the areas that are covered by at least 15% ice—and the
 87 ice thickness typically reaches its peak around March. Starting in
 88 late spring, ice melting gradually exceeds water freezing due to
 89 higher temperatures and longer hours of sunlight exposure. Sea ice
 90 typically reaches the minimum extent and thickness in
 91 mid-September, when ice coverage can drop to under half of the
 92 winter maximum.³⁴ After mid-September, sea water freezing starts
 93 to exceed ice melting, so ice coverage expands. This cycle repeats
 94 annually.

95 Albedo, the percentage of incident light reflected from the
 96 surface of the earth, is highly dependent on the ice extent.³⁵ Light-
 97 colored ice or snow reflects more light than blue-colored liquid
 98 water; therefore, ice is essential to keeping the Arctic at a cooler
 99 temperature and subsequently maintaining the energy balance
 100 around the globe. If the energy balance is broken, as ice decline has
 101 been detected in recent years, the ice-albedo feedback loop effect
 102 may occur, i.e., less reflection and more absorption of solar energy,
 103 leading to even more ice loss and further global warming. Moreover,
 104 the Arctic ecosystem is directly impacted by the change in sea ice
 105 coverage, which, for instance, threatens the lives of polar bears and
 106 walruses who rely on sea ice for hunting and breeding.³⁶

107 Data recorded by the National Aeronautics and Space
 108 Administration (NASA) and the National Snow and Ice Data
 109 Center (NSIDC) since 1979 has shown substantial declines in both
 110 ice extent and thickness in the Arctic, despite the year-over-year
 111 fluctuations in either direction. The lowest Arctic sea ice extent was
 112 observed in September of 2012^{1,37}; between 2013 and 2022, the ice
 113 extent was higher than the 2012 minimum, but still much lower
 114 than the average of the past four decades. July 2023 was reported as
 115 the hottest month of the earth on record,³⁸ and 2023, the hottest
 116 year by a significant margin.^{3,39} Some questions then come to us
 117 naturally: how does the Arctic sea ice extent in 2023 compare to the
 118 2012 level? And, can our model simulations closely match the
 119 observations in the real data? These questions will be addressed in
 120 Sec. V D.

II. THEORETICAL FRAMEWORK

121

A. Classical Ising model

122

The system described by an IM is a set of lattice sites, each
 having a spin that interacts with its neighbors. The Hamiltonian
 function^{4,5,10} for the lattice σ in a standard IM is given as

$$H(\sigma) = - \sum_{\langle i,j \rangle} J_{ij} \sigma_i \sigma_j - \sum_i B_i \sigma_i, \quad (1)$$

where σ_i represents the spin variables at site i and takes the value
 of +1 or -1; J_{ij} represents the interaction between sites i and j and
 can take positive values for ferromagnetic and paramagnetic mate-
 rials, or negative for antiferromagnetic materials; and B_i captures
 the interaction between the external field and site i . i and j range
 across the full lattice, which can be one, two, or higher dimensions,
 and $\langle i, j \rangle$ represents pairs of spins at sites i and j that interact with
 each other. In a simple setup, each spin may only interact with its
 nearest neighbors, so $\langle i, j \rangle$ sums over adjacent sites only. For
 example, in a simple 2D IM, each spin interacts only with the sites
 positioned immediately left, right, above, and below.

In statistical physics, the configuration probability of lattice σ
 follows the Boltzmann distribution:⁴⁰

$$P_\beta(\sigma) = \frac{e^{-\beta H(\sigma)}}{Z_\beta}, \quad (2)$$

where Z_β is the partition function,

$$Z_\beta = \sum_{\sigma} e^{-\beta H(\sigma)} \quad (3)$$

and

$$\beta = (k_B T)^{-1}. \quad (4)$$

β is the inverse temperature; k_B is the Boltzmann constant;
 and T is the IM temperature, which differentiates from the ambient
 temperature discussed later.

The evolution of the kinetic IM runs through a series of spin
 flips over the lattice. The probability of each flip depends on
 whether it increases or reduces the Hamiltonian of the system.
 Mathematically, the probability is determined by $\min(1, e^{-\beta(H_v - H_u)})$,⁴¹
 where H_v and H_u represent the Hamiltonian of the system before and
 after the flip. We can easily see that higher IM temperatures lead to
 greater thermal fluctuations and larger variances in the spin value dis-
 tribution, while lower IM temperatures result in fewer fluctuations.

B. Continuous spin Ising model

153

Most of the Ising literature cited in earlier sections^{5,10,21,28,29} focus on binary values of the spins, i.e., σ_i taking values of +1 or -1 only. However, the sea ice data for each location takes varying values between 0 and 1 that represent the percentage of ice coverage. Therefore, we generalize the IM to allow for continuous spin values that can take any real number between -1 and +1. This generalization enables the IM to examine more realistic systems but

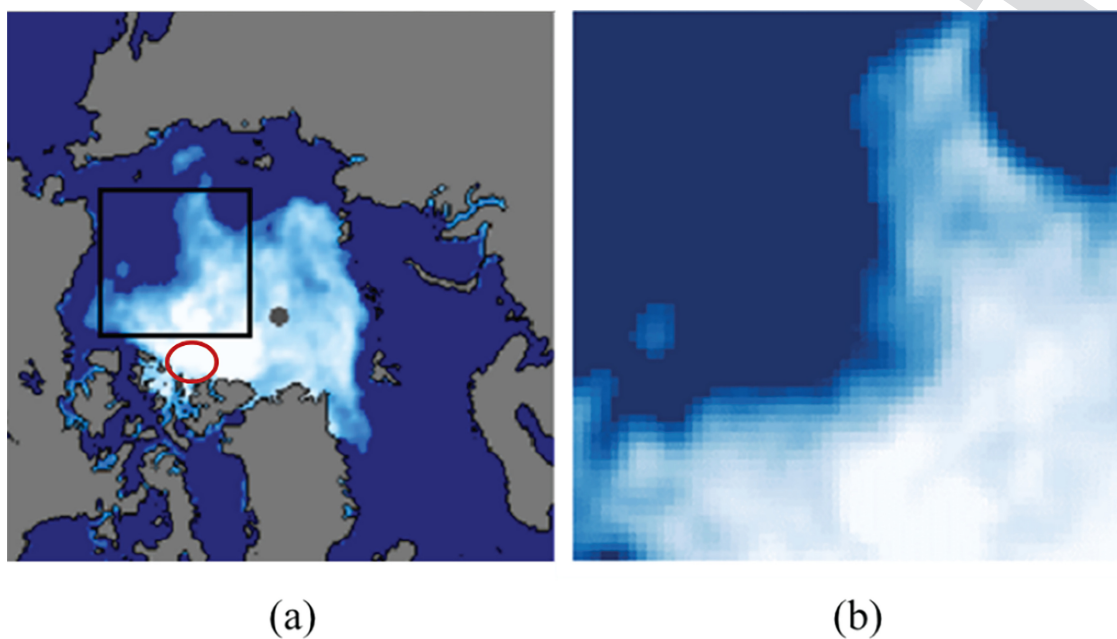
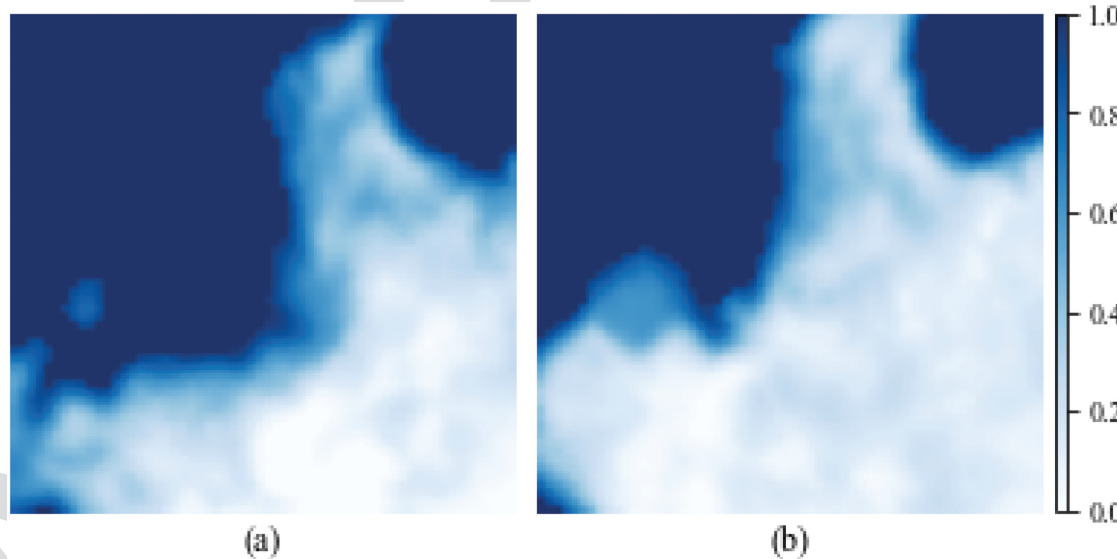


FIG. 1. (a) Part of the NRTSI data on September 16 2022, where the black square marks the focus area for this study and red oval the Canadian Arctic Archipelago area with the thickest ice.⁴³ (b) A zoom-in view of the focus area, a 60×60 square lattice covering approximately 2.25 million square kilometers.



Q10

FIG. 2. The initial and the final target states of an IM lattice simulation run. (a) shows the actual configuration observed in our focus area on September 16 2022 and (b) on October 1 2022. Each full simulation period is half a month. Blue color indicates water; white indicates ice. The darker the color of each cell, the higher the water concentration and the lower the ice coverage, as shown by the color scale on the right.

also adds a high degree of complexity to the mathematical solutions. Past research has studied phase transitions and critical behaviors of the continuous IM.^{6,7} Recently, an IM with variable power-law spin strengths is studied with its rich phase diagrams.⁴²

The Hamiltonian function of the continuous spin IM is represented by the same Eq. (1). However, σ_i now takes continuous values between +1 and -1; $-J_{ij}\sigma_i\sigma_j$ reaches the minimum energy state if $\sigma_i = \sigma_j = +1$, or $\sigma_i = \sigma_j = -1$, as the energy of any other value pair is higher. The highest energy is observed when $\sigma_i = +1$, $\sigma_j = -1$, or vice versa. This numeric feature works ideally for an ice/water lattice: the most stable low energy state is either 100% water or ice across two adjacent locations, whereas full ice next to full water displays the most unstable high energy state.

C. Monte Carlo simulation and inertia factor

The introduction of the continuous spins also adds to the complexity of the Monte Carlo (MC) simulation of the Ising lattice. In the classical binary-spin IM, σ_i can only flip to $-\sigma_i$; and, therefore, the absolute value of the change is always 2 no matter if the flip goes from -1 to +1 or vice versa. In a continuous spin IM, the challenge of determining a post-flip spin value nevertheless arises.

In our approach, this new spin value is implemented through a random number σ'_i uniformly distributed between -1 and +1, which will be explained in greater details in Sec. IV D. Moreover, we incorporate an innovative inertia factor I , and the probability of each flip is determined by

$$P_{\text{flip}} = \min(1, e^{-\beta(H_v - H_\mu + I|\sigma'_i - \sigma_i|)}), \quad (5)$$

where σ_i represents the original spin value before the change, σ'_i the new attempted value, and H_v and H_μ the system Hamiltonian before and after as described in Eq. (1) and Sec. II A.

The newly added $-I|\sigma'_i - \sigma_i|$ accounts for the energy needed to overcome the inertia of the spin change, and I is an IM parameter to be fitted. Intuitively, this term represents the natural resistance to any state change and can also be thought of as an analog to the latent heat needed for the ice/water phase transition in classical thermodynamics. Motivated by the fact that the total energy change for water/ice phase transition at constant temperature and pressure is proportional to mass, we choose a linear functional form for the inertia term as the simplest and most sensible assumption. Therefore, the total energy change required for a spin flip is

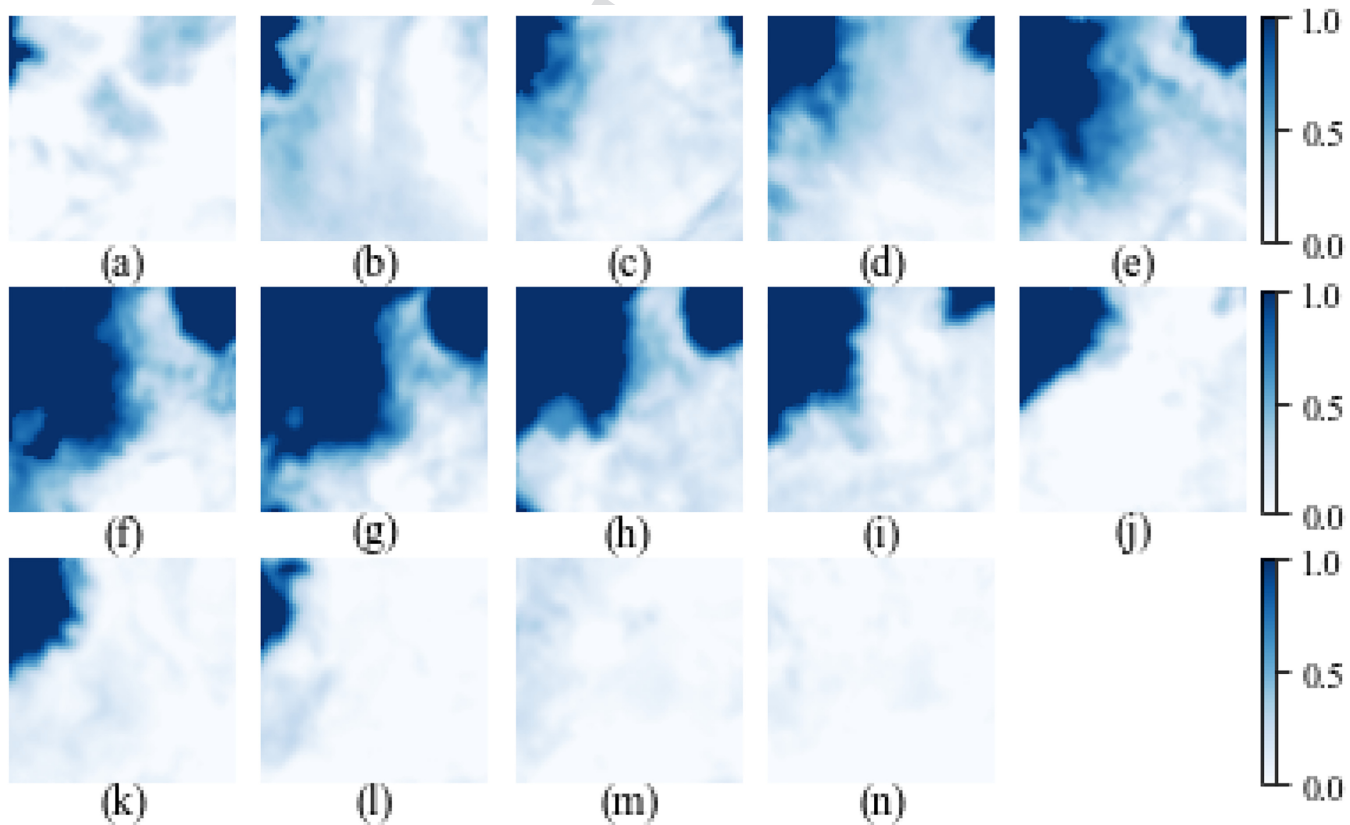


FIG. 3. The actual semi-monthly sea ice evolution in the focus area in 2022: (a) June 16, (b) July 1, (c) July 16, (d) August 1, (e) August 16, (f) September 1, (g) September 16, (h) October 1, (i) October 16, (j) November 1, (k) November 16, (l) December 1, (m) December 16 2022, and (n) January 1 2023.

TABLE I. The best-fit Ising parameters for the 2022 sea ice evolution.

	6/16– 7/1	7/1–7/ 16	7/16– 8/1	8/1–8/ 16	8/16– 9/1	9/1–9/ 16	9/16– 10/1	10/1– 10/16	10/16– 11/1	11/1– 11/16	11/16– 12/1	12/1– 12/16	12/16–1/1/ 2023
J	2.3	2.6	2.3	2.4	2.7	2.3	2.6	2.7	2.6	2.5	2.3	2.7	2.7
B_0	7.0	2.0	6.5	9.1	4.3	3.6	-12.6	-12.7	-14.9	-9.6	-15.0	-13.1	-14.4
B_x	0.2	-9.7	-5.5	3.7	-7.5	-8.2	-10.0	-6.1	-8.5	9.7	-1.9	-0.8	-3.1
B_y	-10.0	3.0	3.7	1.0	-6.4	2.9	0.1	-8.4	-5.6	-10.0	-5.9	5.4	-8.0
I	10.3	9.1	11.0	10.8	10.7	10.9	10.6	9.3	9.4	10.4	9.1	10.9	10.8

199 $\Delta E = H_v - H_\mu + I|\sigma'_i - \sigma_i|$, which consists of two parts: the system
200 Hamiltonian change plus the inertia term. The probability of spin
201 value change follows the Boltzmann distribution as Eq. (5).

202 Here is an example to illustrate the inertia effect. Starting with
203 an initial spin value of 0.8, a flip to either 0.7 or 0.6 may result in
204 the same system Hamiltonian. However, we differentiate these two
205 new states by assigning higher probability for the flip to 0.7 because
206 of the smaller spin change. In Eq. (5), $-I|\sigma'_i - \sigma_i|$ influences the
207 distribution of the new spin values, and in practice, it significantly
208 improves the simulation results to better match the observations.

In summary, we introduce a novel inertia factor to the continuous spin IM. These mathematical additions prepare us to study real-world Arctic sea ice dynamics while keeping the computational complexity tractable.

III. DATA DESCRIPTION

Our study uses the “Near-Real-Time DMSP SSMIS Daily Polar Gridded Sea Ice Concentrations” (NRTSI) data set⁹ collected by the National Snow and Ice Data Center (NSIDC), which

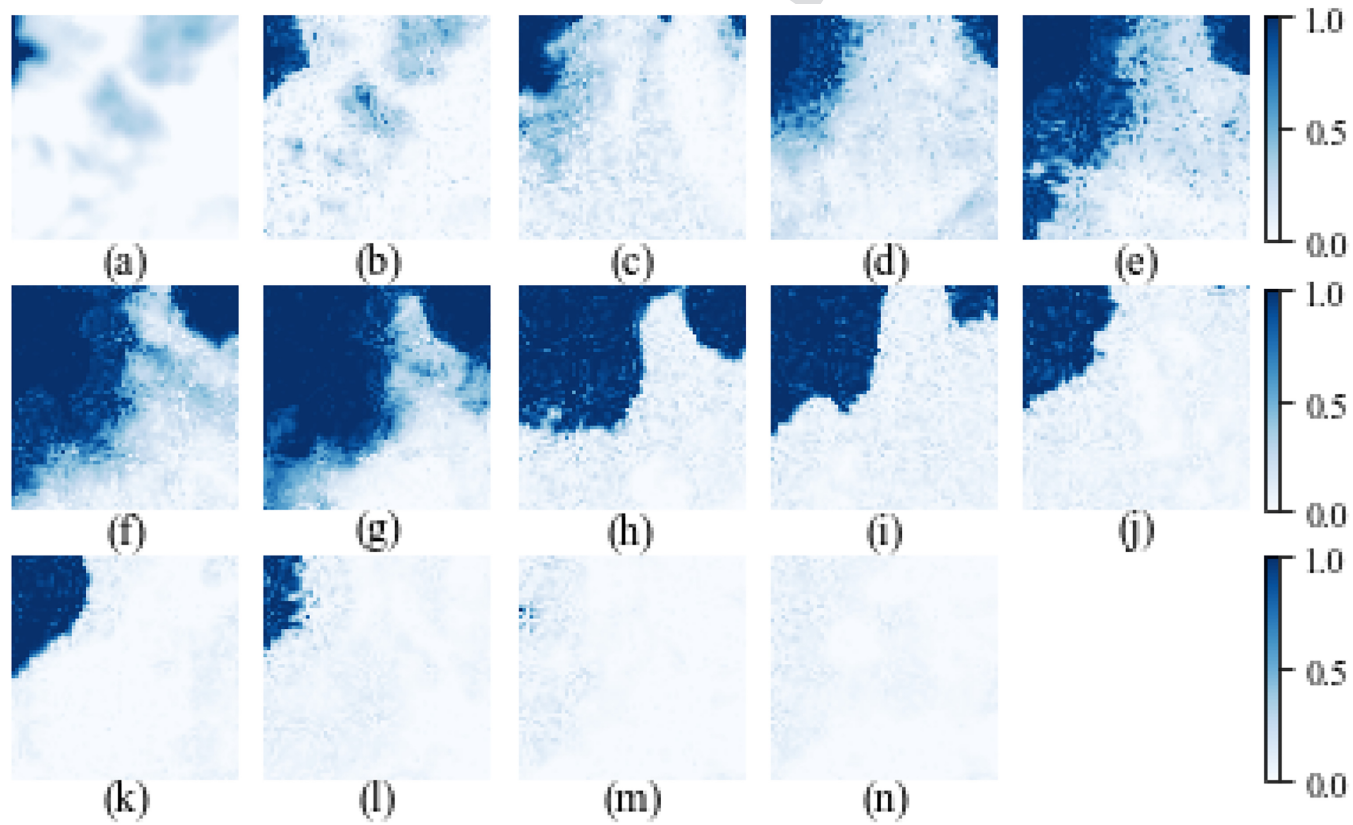


FIG. 4. The simulated semi-monthly sea ice evolution in the focus area in 2022. (a) is the actual image on June 16 2022 as the start state; (b)–(n) are simulated images on (b) July 1, (c) July 16, (d) August 1, (e) August 16, (f) September 1, (g) September 16, (h) October 1, (i) October 16, (j) November 1, (k) November 16, (l) December 1, (m) December 16, and (n) January 1 2023.

captures daily sea ice concentrations for both the Northern and Southern Hemispheres. The Special Sensor Microwave Imager/Sounder (SSMIS) on the NANA Defense Meteorological Satellite Program (DMSP) satellites acquires the near-real-time passive microwave brightness temperatures, which are inputted into the NRSTI data set using the NASA Team algorithm to generate the sea ice concentrations.

The NRSTI files are in netCDF format. Each file of the Arctic region contains a lattice of 448 rows by 304 columns, covering a large earth surface area with the north pole at the center. Each grid cell represents an area of approximately 25 by 25 km. The value for each grid cell is an integer from 0 to 250 that indicates the fractional ice coverage scaled by 250, with 0 indicating 0% ice concentration and 250 for 100% ice concentration. The image of part of the NRSTI file on September 16 2022 is illustrated in Fig. 1(a). In the map, white represents ice, blue represents water, and gray represents land. The exact location of the north pole is covered by a gray circular mask because of the limitation of the satellite sensor measurement caused by the orbit inclination and instrument swath. The red oval marks the Canadian Arctic Archipelago area with the thickest ice,⁴³ which is worth of some discussions later in the paper.

For this research, we focus on studying a specific geographic region bounded by the black square in Fig. 1(a), ranging from the East Siberian Sea (to the top of the box) and the Beaufort Sea (to the left) to near the polar point; a zoom-in image of this focus area is shown in Fig. 1(b). This large square area is unobstructed by land or the north pole mask, making it ideal for the IM lattice setup. This area corresponds to 60 rows and 60 columns in the data file, covering approximately $1500 \times 1500 \text{ km}^2$ or about 2.25×10^6 square kilometers.

IV. ISING LATTICE AND SIMULATION SETUP

The methodology of our study on sea ice dynamics is outlined as follows. We first normalize the NRSTI data to a continuous Ising lattice, carefully choose the simulation periods, and set up the Ising parameters (J , B , I) to be fitted. Then given the initial lattice of each simulation period, we run the Metropolis MC simulation based on the values of (J , B , and I) to generate a final state of the Ising lattice for this period. The full Metropolis simulation procedure is passed into a numeric optimizer to find the best-fit Ising parameters so that the simulated final Ising lattice matches the observed NRSTI data as closely as possible.

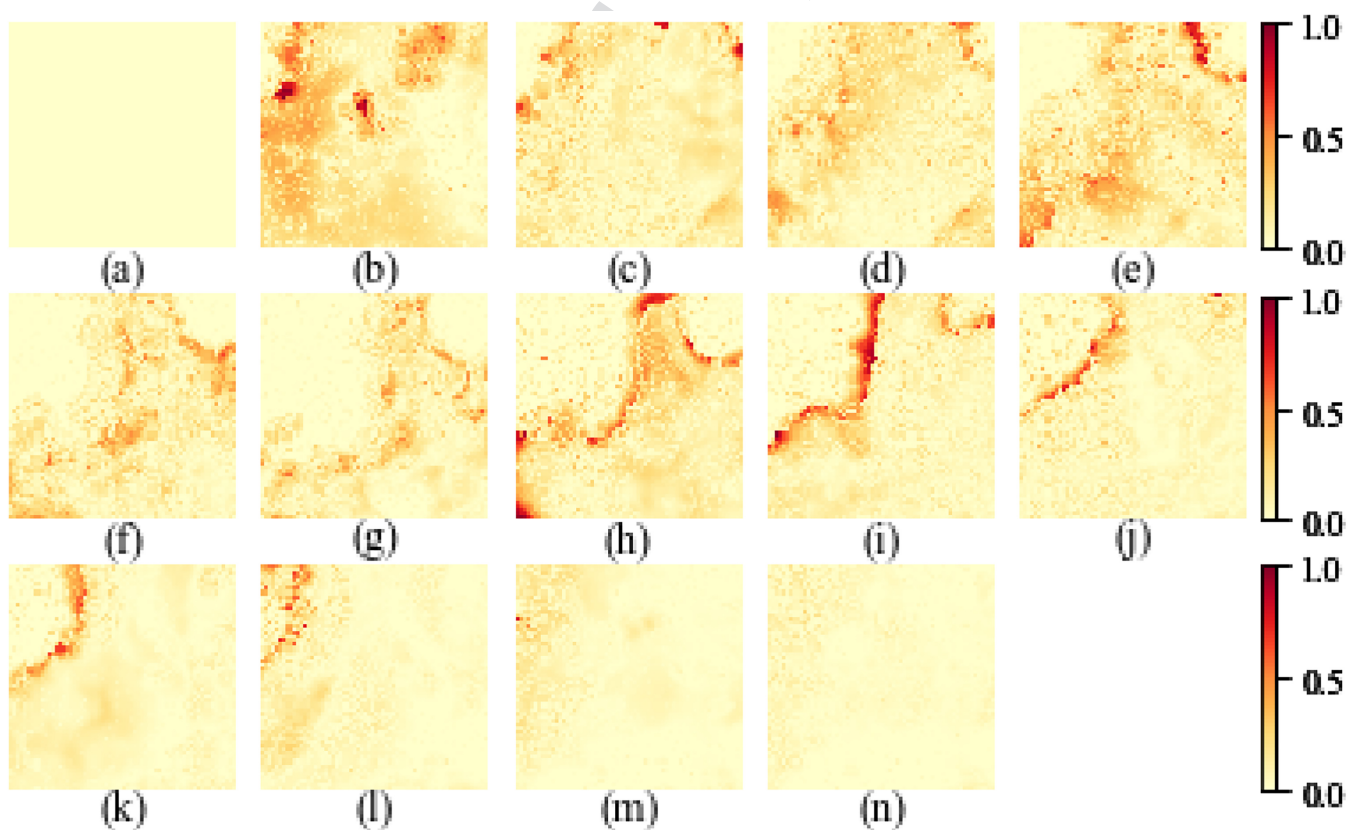


FIG. 5. Heatmaps illustrating the absolute difference (between 0 and 1) in ice coverages between Figs. 3 and 4 for each semi-monthly period from (a) June 16 2022 to (n) January 1 2023. Yellow color indicates a good match and red a large difference, as shown by the scale on the right.

257 **A. Ising lattice**

258 We start with a transformation of the NRTSI data of the focus
 259 region shown in Fig. 1(b) to the Ising-style data. A simple linear
 260 mapping is applied to convert integers from 0 to 250 to real
 261 numbers from -1 to $+1$. -1 indicates that a location cell is 100%
 262 ice, $+1$ indicates 100% water, and 0 indicates 50%/50% coverage of
 263 water/ice. Each cell covers $25 \times 25 \text{ km}^2$ of the total $1500 \times 1500 \text{ km}^2$
 264 focus region, and, therefore, a 60×60 matrix is initialized for the
 265 2D IM lattice in our study.

266 **B. Simulation periods**

267 Figures 2(a) and 2(b) display an example of the initial and the
 268 final target states of an IM lattice simulation run. The simulation
 269 periods are chosen to be consistently half a month apart, for
 270 example, September 16 2022 in Fig. 2(a) and October 1 2022 in
 271 Fig. 2(b). This semi-monthly frequency is chosen to balance two
 272 considerations. First, the period is sufficiently long to allow for
 273 sizable differentiation in the ice/water configurations between the
 274 start and the end dates and second, the period is not too long and
 275 allows the IM simulation to mimic the daily ice/water evolution on
 276 the interim dates between the start and the end, which is to be
 277 illustrated in Sec. V B.

278 **C. Ising model parameters**

279 In the IM Hamiltonian function, i.e., Eq. (1), we set the
 280 following:

- σ_i is a real number between -1 and $+1$ for any cell i in our focus area. 281
 \square 282
- $a_{i,j}$ sums over four adjacent cells positioned immediately left, right, above, and below. 284
 \square 285
- J_{ij} is set to be constant within each simulation period across all cells. 286
 \square 287
- B_i is set to be time-invariant within each simulation period. 288
 \square 289 However, in order to capture the variations in the external forces due to the environmental differences across geographic locations, 290 B_i is set to be a linear function of x_i and y_i coordinates (the row 291 and the column of cell i in the Ising lattice respectively), i.e., 292 $B_i = B_0 + B_x(x_i - x_0) + B_y(y_i - y_0)$, where B_0 is the value of B at 293 the lattice center with coordinates x_0 and y_0 . 294
- I , the inertia factor, is set to be constant within each simulation period. 295
 \square 296
- β , the inverse Boltzmann temperature, is set to 1. In this study, what matters is the relative magnitudes of (J , B_0 , B_x , B_y , and I) instead of their individual absolute values, so we can set β to 1 without loss of generality. A similar approach has been taken in other kinetic Ising model research.²⁸ 297
 \square 298

302 **D. Metropolis simulation steps**

303 Various MC methods have been developed for the IM simulation. Among them the most widely used are the Glauber dynamics⁴⁴ 304 and the Metropolis-Hastings algorithm.⁸ In our study, we follow the 305 latter for the MC simulation of the IM lattice evolution. As described 306

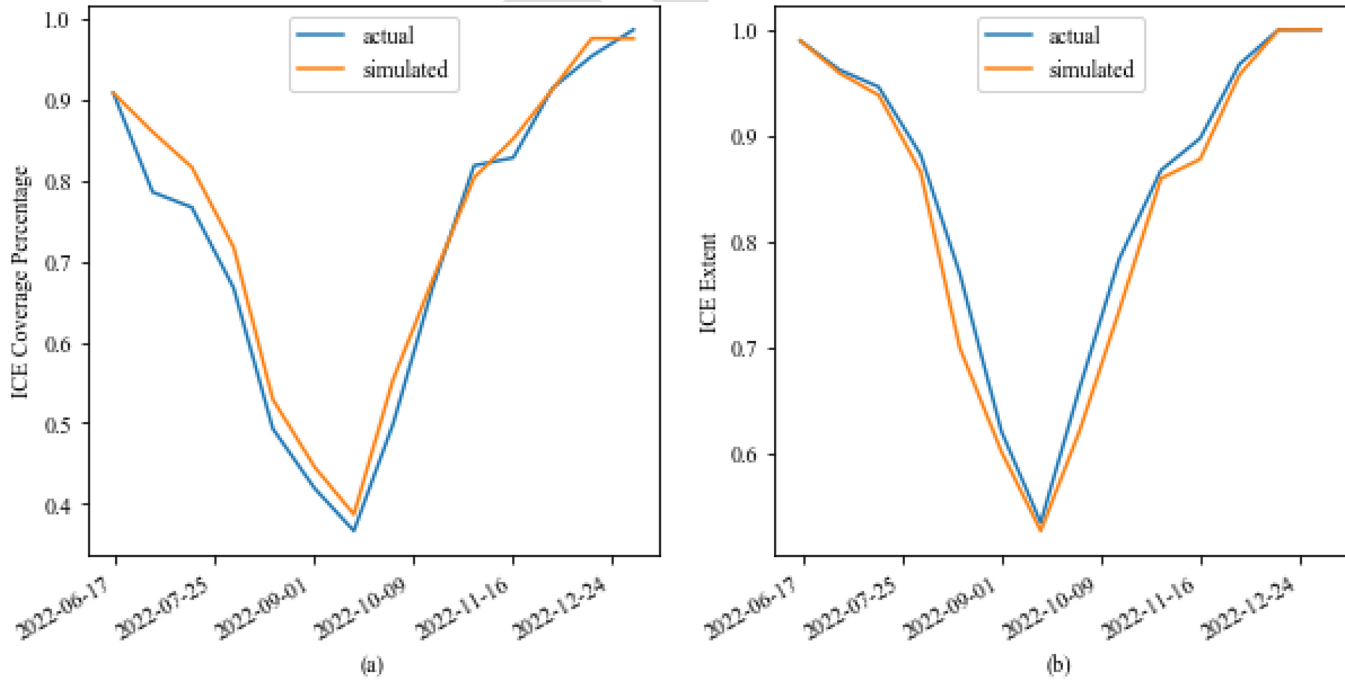


FIG. 6. (a) The ice coverage percentage (the average of ice coverages) in the focus area from June 16 2022 to Jan 1 2023. (b) The sea ice extent (the percentage of areas with at least 15% ice coverage) for the same period. Blue curves are the actual measures from the NRTSI data; orange ones show the IM simulation results.

307 in Sec. II C, an inertia factor is introduced into our model and the
 308 generalized Metropolis-Hastings MC steps are listed below.

- 309 1. Select cell i at random from the 2D lattice of the focus area. Let
 310 the spin value of this cell be σ_i .
- 311 2. Generate another uniform random variable σ'_i between -1 and
 312 $+1$.
- 313 3. Compute the energy change $\Delta H_i = H_v - H_\mu$ from σ_i to σ'_i .
- 314 4. Compute the energy $I|\sigma'_i - \sigma_i|$ to overcome the inertia of
 315 changing the spin value at i .
- 316 5. Compute the total energy change $\Delta E = \Delta H_i + I|\sigma'_i - \sigma_i|$.
- 317 6. (a) If ΔE is negative, the energy change is favorable since the
 318 energy is reduced. The spin value change is, therefore, accepted
 319 to σ'_i .
- 320 7. If ΔE is positive, the probability of the spin flip is determined by
 321 the Boltzmann distribution. In this case, another uniform

random variable r between 0 and 1 is generated. If r is less than 322
 $P = e^{-\beta \Delta E}$, the spin value change is accepted; otherwise, the 323
 change is rejected and the spin value at i stays at σ_i . 324

For each semi-monthly simulation period, we repeat the above 325
 MC steps 50 000 times. As the lattice of our focus area has 3600 326
 cells, this repetition allows for approximately 14 flip tries for each 327
 cell, or roughly once per day. This specific repetition number is 328
 chosen by taking into account the computational complexity of the 329
 algorithm and also making sure that each cell of the Ising lattice 330
 gets sufficient attempts to be changed. Other choices of the repeti- 331
 tion number can be considered, which may result in different fitted 332
 parameter values. What is important is to ensure the number of 333
 repetitions for each period proportional to its duration, so the time 334
 unit of each Metropolis step is the same across the full simulation 335
 process.²⁸ 336

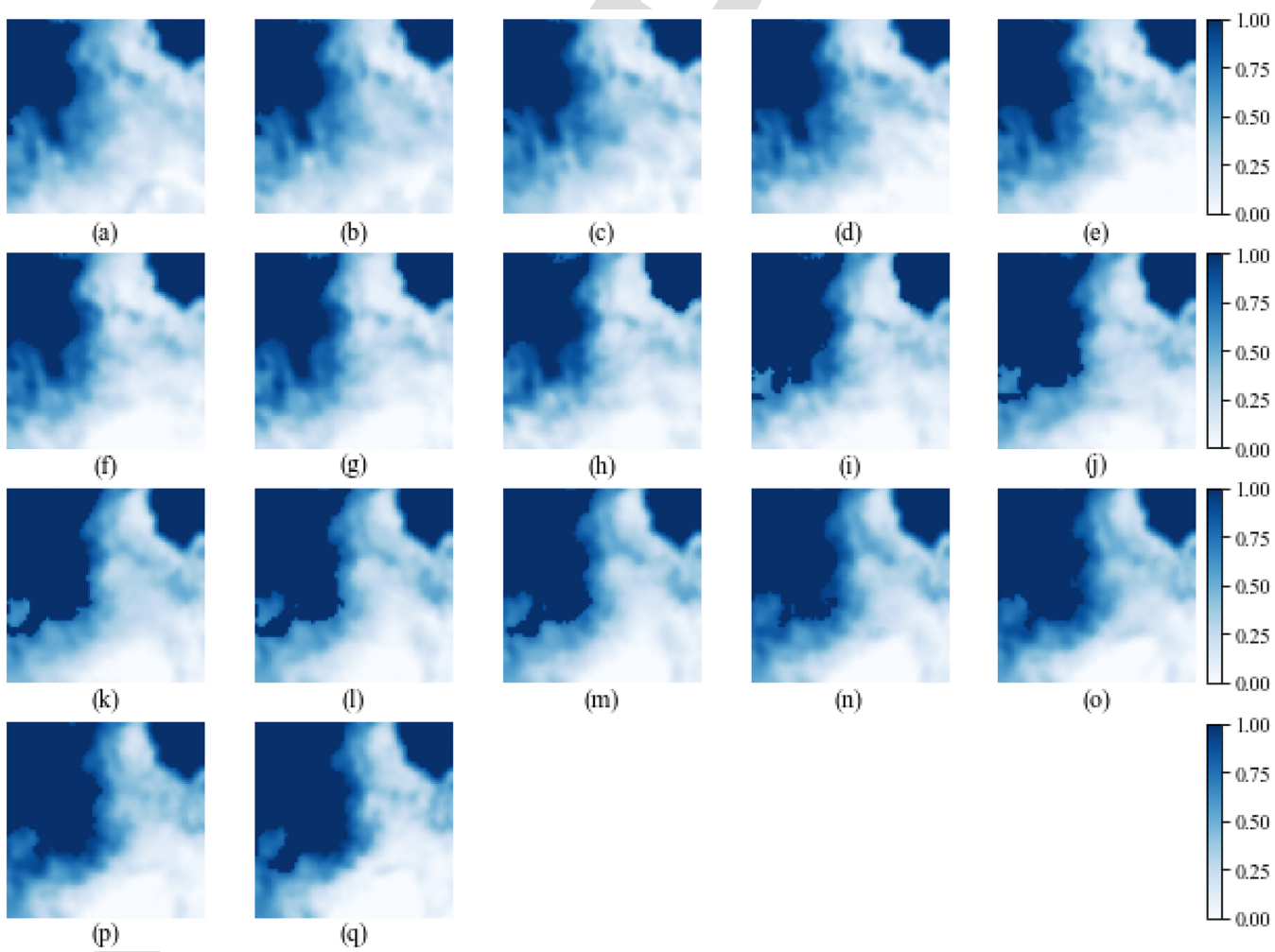


FIG. 7. The actual daily sea ice evolution in the focus area during a melting cycle from (a) August 16 to (q) September 1 2022.

337 E. Dual annealing optimization

Q2 338 As described in Sec. IV D, the Ising parameters (J , B_0 , B_x , B_y and I) dictate the sea ice evolution process in the Metropolis MC simulations, and, therefore, different parameter regimes shall lead 339 to varying final states. With the goal to match the observed final 340 state lattice configuration as closely as possible upon the completion of 341 the simulations, we measure the similarity between the observed and 342 the simulated final lattice configurations by the sum of the absolute 343 spin value differentials across the lattice. Mathematically, this is 344 the Manhattan distance (as opposed to the more commonly used 345 Euclidean distance) between the observed and the simulated matrices. 346 We then fit the values of parameters (J , B_0 , B_x , B_y , and I) to maximize 347 of the similarity measure, i.e., to minimize the sum of the absolute 348 spin value differentials. The minimization is done with the dual 349 annealing optimization method, which combines classical simulated 350 annealing with a local search to achieve the global minimization solution. 351 Description of the dual annealing method can be found in 352 the Python SciPy package. 353

annealing with a local search to achieve the global minimization solution.³⁵²
³⁵³ Description of the dual annealing method can be found in
³⁵⁴ the Python SciPy package.

V. RESULTS

355

We employ the continuous spin IM to simulate the dynamics 356 of the sea ice/water transition for the focus Arctic Sea area. Thanks 357 to the NRTSI data, we can conduct the simulation for every year in 358 the past four decades. 359

A. Simulation results for 2022

360

Figure 3 shows the actual semi-monthly sea ice images in our 361 focus area from 16 June 2022 to 1 January 2023. As can be seen, 362 the melting cycle starts from June 16 and goes until September 16, 363

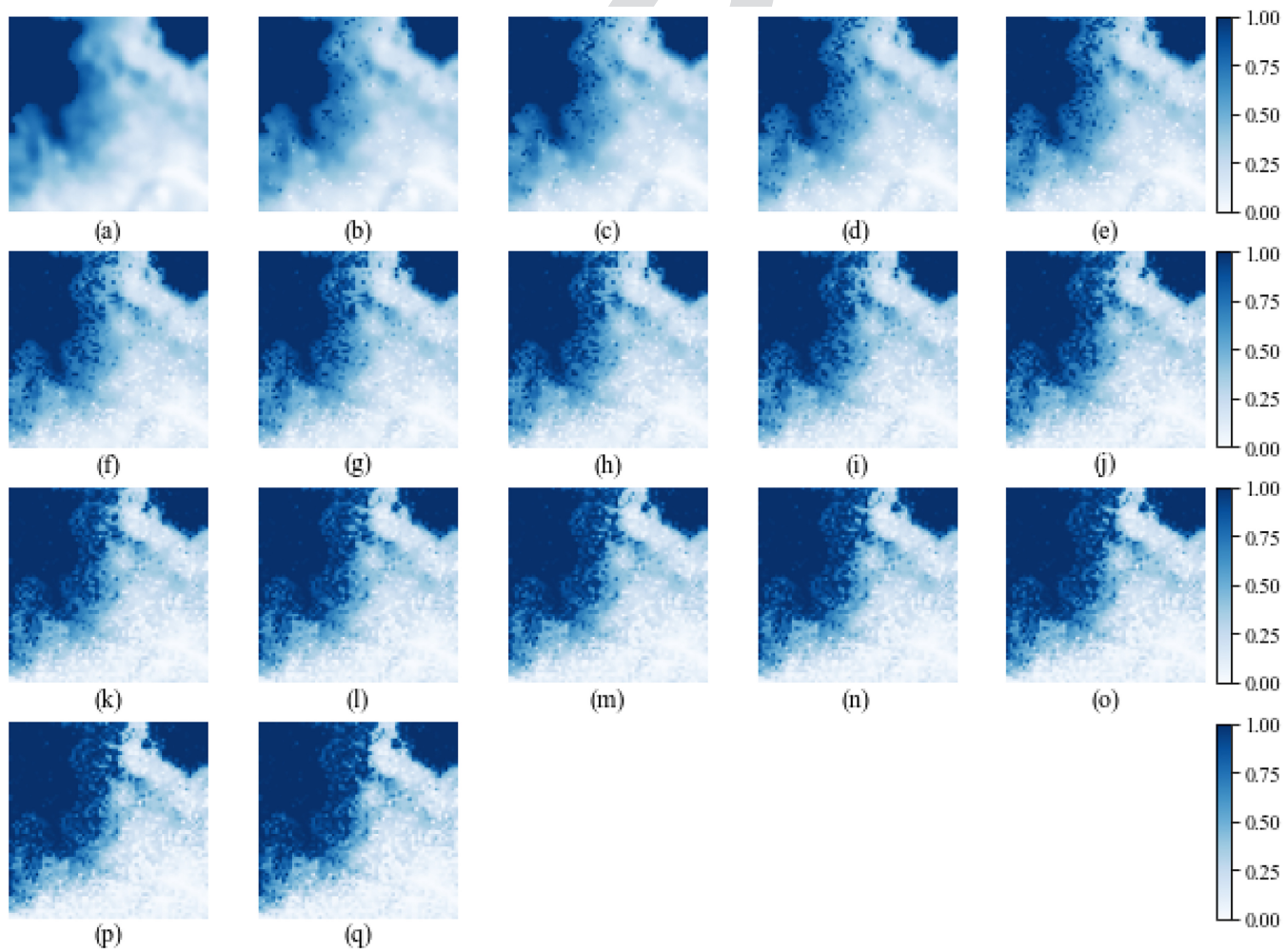


FIG. 8. The simulated daily sea ice evolution, based on the semi-monthly Ising parameters, in the focus area during a melting cycle from (a) August 16 to (q) September 1 2022.

and the freezing cycle from September 16 to year end. Prior to June 16, the region is almost fully covered by ice, so the IM simulation will be trivial. This is why we set the simulation start date on June 16 of each year. During the period of June 16 to December 16, every successive image shows considerable ice coverage difference from the previous date while retaining certain core features. This semi-monthly frequency choice allows our IM simulation to capture the essence of the evolution dynamics without overfitting the model.

The best-fit Ising parameters (J , B_0 , B_x , B_y , and I) for each simulation period in 2022 are shown in Table I. The spin interaction coefficient J and the inertia factor I are relatively stable; intuitively, the strength of such interactions does not change much across different time periods. Moreover, J remains positive across all periods, confirming that adjacent cells are inclined to maintain values of the same sign, i.e., the area surrounding ice will be

more likely to freeze, and that surrounding water will tend to melt. In this sense, the ice/water system displays the feature of ferromagnetism/paramagnetism instead of antiferromagnetism.

On the other hand, the external force parameters B_0 , B_x , and B_y display large variations across different time periods. In particular, the average force B_0 is positive from June 1 to September 16 but turns negative afterward, which can be explained by the seasonal ambient temperature as the dominant external factor for ice/water dynamics. Ambient temperature is not the only factor, though. Arctic temperature normally peaks in July/August while B_0 remains positive and ice melting continues through mid-September. This lag effect could be explained by other environmental effects such as albedo or jet streams but is beyond the scope of this study.

The values of B_x and B_y are mostly negative due to the geographic distribution of ice coverage. For our Ising lattice representing the focus area, x coordinates corresponding to the rows of the

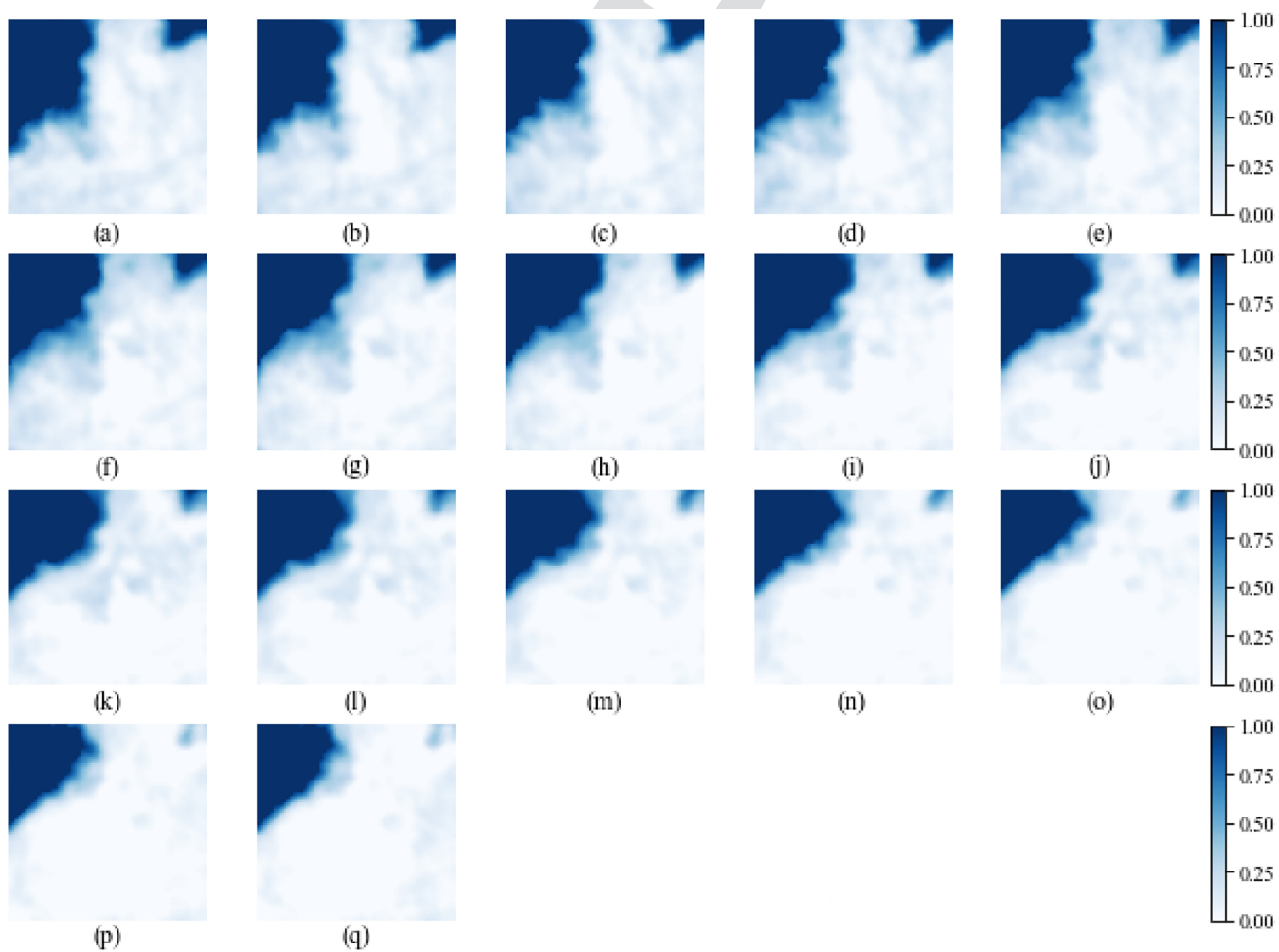


FIG. 9. The actual daily sea ice evolution in the focus area during a freezing cycle from (a) October 16 to (q) November 1 2022.

396 lattice increase from top to bottom; y coordinates for the columns
 397 increase from left to right. Interestingly, ice coverage near the
 398 bottom of our area, the Canadian Arctic Archipelago marked by
 399 the red oval in Fig. 1, is much thicker than elsewhere including the
 400 north pole (the gray circular mask). In fact, many scientists believe
 401 this region will have the last piece of ice standing in the Arctic if
 402 the Blue Ocean Event happens.⁴³ As the lower part of the focus
 403 area tends to have greater ice coverage, B_x is mostly negative, except
 404 for very few periods when the ice coverage remains relatively
 405 unchanged. B_y is less negative, as the impact of the geographic loca-
 406 tion along the y direction is less pronounced than that of x because
 407 the ice at the north pole is thinner than in Archipelago, which miti-
 408 gates the impact of the y coordinate of a cell. In addition, the
 409 values of B_x and B_y exhibit greater fluctuations than other parame-
 410 ters, indicating that our simplified linear functional form of

$B_i = B_0 + B_x(x_i - x_0) + B_y(y_i - y_0)$ is far from perfectly modeling the full effect of external fields; it can be further enriched by linking to actual geographical and environmental factors to enhance the power of the Ising model, which is left for our future research.

The simulated sea ice images for each 2022 period are shown in Fig. 4 utilizing the best-fit Ising parameters in Table I. These images exhibit excellent similarity to Fig. 3, demonstrating the strong explanatory power of our Ising model. Nevertheless, upon close inspection, the images in Figs. 3 and 4 do reveal discrepancies, especially as shown in images [(e) for August 16, (h) October 1, and (i) October 16 2022, respectively], where the ice image display significant irregularity compared to the prior period. While an IM with simple parameterization encounters difficulties in describing these local irregularities, it is feasible to include a richer

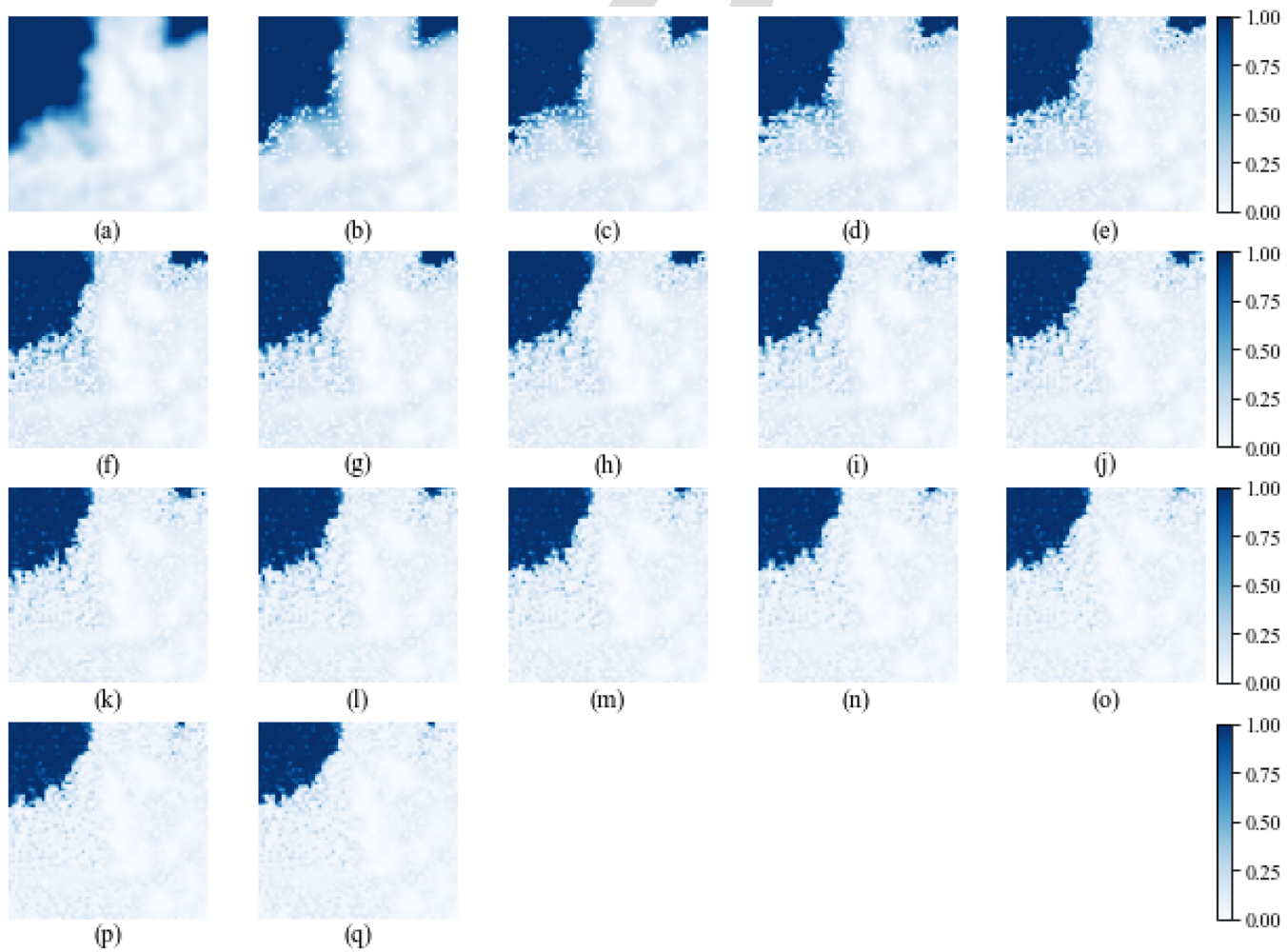


FIG. 10. The simulated daily sea ice evolution, based on the semi-month Ising parameters, in the focus area during a freezing cycle from (a) October 16 to (q) November 1 2022.

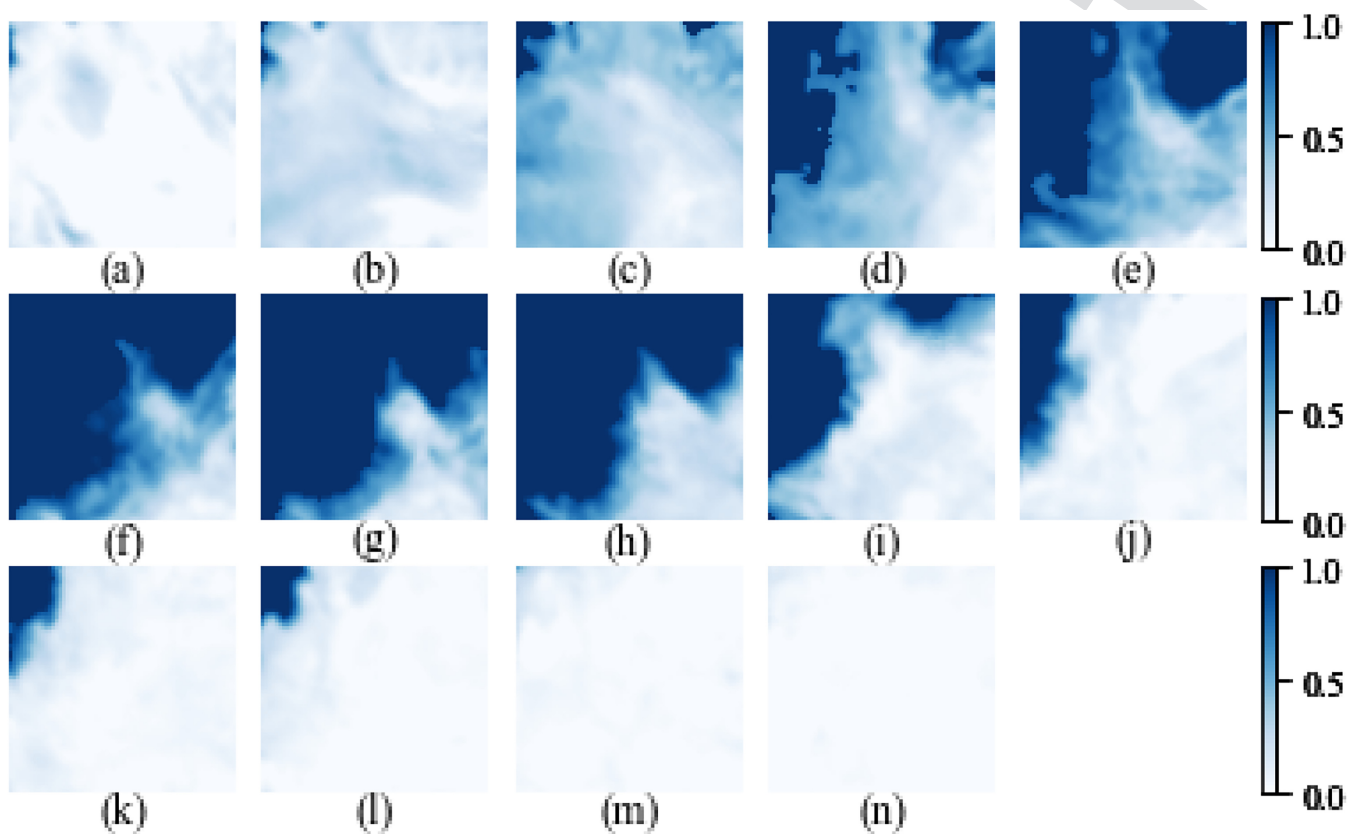


FIG. 11. The actual semi-monthly sea ice evolution in the focus area in 2023: (a) June 16, (b) July 1, (c) July 16, (d) August 1, (e) August 16, (f) September 1, (g) September 16, (h) October 1, (i) October 16, (j) November 1, (k) November 16, (l) December 1, (m) December 16, and (n) January 1 2024.

426 set of parameters or to employ more complicated parametric func-
 427 tional forms at the potential cost of overfitting. In this paper,
 428 we keep our Ising model tractable and accept these local
 429 discrepancies.

430 To quantify the similarity between the IM simulated configu-
 431 rations and the observed images, the absolute difference in ice
 432 coverages across the entire focus area for each of the simulation
 433 period in Figs. 3 and 4 are calculated; the results are illustrated as
 434 the heatmaps in Figs. 5(a)–5(n), where light yellow color indicates

435 that the actual and the simulated images match well, whereas red 436 patches are associated with the locations that display large dis- 437 crepancy. The heatmaps are very revealing: the red patches are 438 consistently small and mostly appear around the boundaries 439 between water and ice, implying that most of the discrepancy 440 between the simulated and actual images happens around these 441 border areas. This is not surprising: the IM needs improvement to 442 perfectly model these boundary granularities, but it does have 443 strong capability to capture the overall patterns. 443

TABLE II. The best-fit Ising parameters for the 2023 sea ice evolution.

	6/16– 7/1	7/1–7/ 16	7/16– 8/1	8/1–8/ 16	8/16– 9/1	9/1–9/ 10/1	9/16– 10/1	10/1–10/ 16	10/16– 11/1	11/1–11/ 16	11/16– 12/1	12/1–12/ 16	12/16–1/1/ 2024
J	2.3	2.3	2.4	2.3	2.3	2.6	2.3	2.7	2.5	2.7	2.4	2.7	2.7
B_0	7.5	7.2	5.2	6.0	7.5	2.6	-1.0	-14.9	-14.7	-12.9	-13.8	-14.7	-15.0
B_x	-0.4	-2.0	-6.7	-7.3	-9.3	-7.3	2.5	-9.5	-4.7	-9.6	-9.3	9.3	-0.3
B_y	-2.0	-3.9	-8.0	5.2	-6.1	-1.8	-9.8	-7.9	-6.3	4.0	-2.4	-3.2	-4.8
I	10.0	10.9	10.8	11.0	10.8	11.0	11.0	10.0	9.5	10.5	9.5	10.5	10.9

Furthermore, we compute two key numerical measures for our focus area: the ice coverage percentage, i.e., the average ice coverages over the lattice, and the ice extent, i.e., the percentage of areas covered by at least 15% ice. [Figure 6](#) compares the actual and the simulated measures; as anticipated, we see an excellent match in both figures as a result of the superior explanatory power of our IM, despite marginal but non-trivial discrepancy. It is interesting to note that the simulated ice coverage percentage is mostly slightly higher than the actual measure, but the simulated ice extent is slightly lower than the actual, a pattern that can be further investigated in future research.

[455 B. Daily sea ice evolution in 2022](#)

Do our semi-monthly IM simulation results match the actual sea ice dynamics on a shorter time scale? To answer this question, we utilize the semi-monthly Ising parameters in [Table I](#) to simulate the daily evolution in 2022. Two periods, a melting period from August 16 to September 1 2022, and a freezing period from October 16 to November 1 2022, are simulated day-by-day for this experiment. The results, with comparisons between the actual and

the simulated daily ice evolution, are shown in [Figs. 7–10](#), respectively. The comparisons exhibit excellent similarity across all the daily images in both periods, confirming that our IM preserves the ice/water dynamics on a shorter time scale.

[467 C. Simulation results for 2023](#)

2023 has witnessed the hottest year on record^{3,39} and is, therefore, a critical year for our study. [Figure 11](#) shows the observed semi-monthly sea ice evolution from June 16 to January 1 in 2024 for our focus area.

Following the same practice as in Sec. V A, IM simulations are conducted for 2023. The best-fit Ising parameters are shown in [Table II](#), the simulated configurations in [Fig. 12](#), and the comparisons for the ice coverage percentage and the ice extent in [Fig. 13](#). Consistent with the 2022 results, excellent match is observed between the IM simulation and the actual sea ice evolution. It is also worth noting that the simulated sea ice extent drops to nearly 30% in September 2023 in our focus area, much lower than the September 2022 level in [Fig. 6](#).

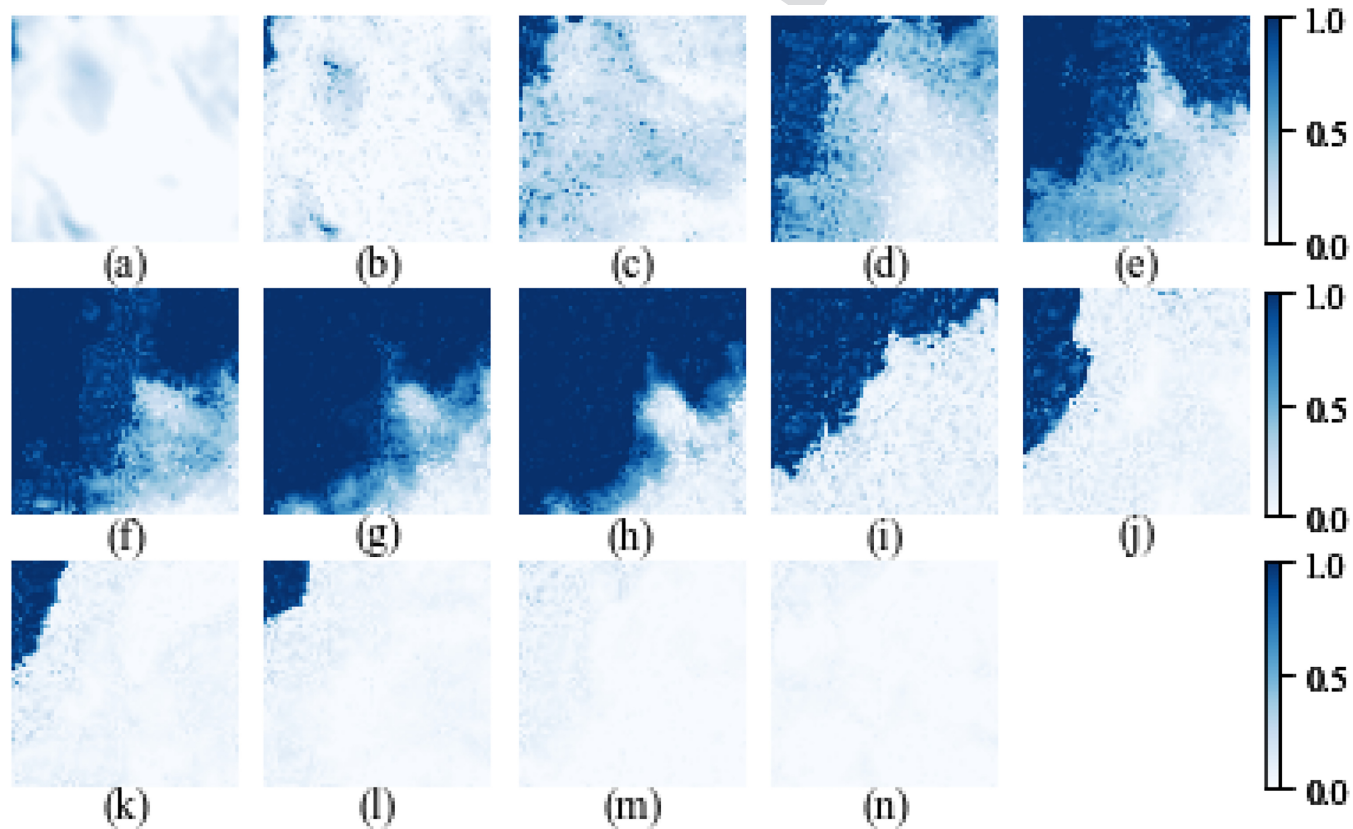


FIG. 12. The simulated semi-monthly sea ice evolution in the focus area in 2023. (a) is the actual image on June 16 as the start state; (b)–(l) are simulated images on (b) July 1, (c) July 16, (d) August 1, (e) August 16, (f) September 1, (g) September 16, (h) October 1, (i) October 16, (j) November 1, (k) November 16, (l) December 1, (m) December 16, and (n) January 1 2024.

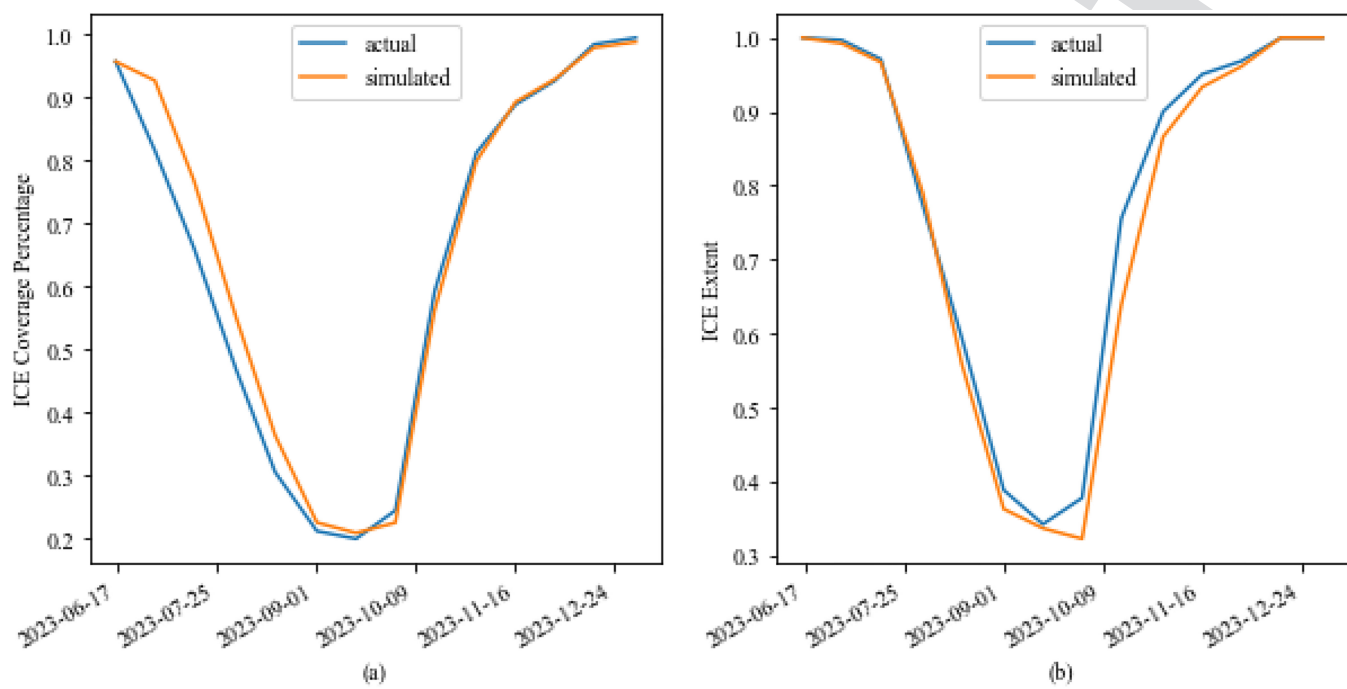


FIG. 13. (a) The ice coverage percentage (the average of ice coverages) in the focus area from June 16 2023 to January 1 2024; (b) The sea ice extent (the percentage of areas with at least 15% ice coverage) for the same period. Blue curves are the actual measures from the NRTSI data; orange ones show the IM simulation results.

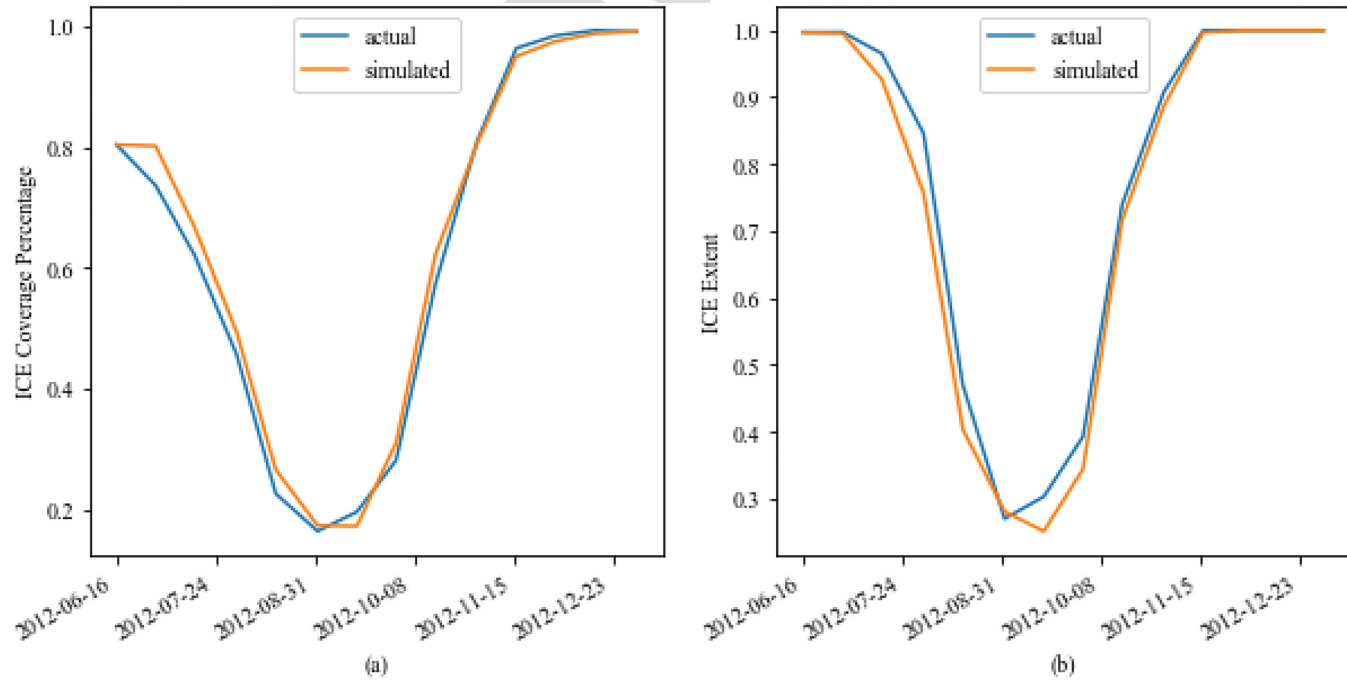


FIG. 14. (a) The ice coverage percentage [(the average of ice coverages)] in the focus area from June 16 2012 to January 1 2013. (b) The sea ice extent (the percentage of areas with at least 15% ice coverage) for the same period. Blue curves are the actual measures from the NRTSI data; orange ones show the IM simulation results.

481 D. Ice extent comparison between 2023 and 2012

482 2012 recorded the lowest September Arctic sea ice extent in
 483 history,² while 2023 witnessed the hottest July and proves to be the
 484 hottest year.^{3,39} It would be an interesting experiment to compare
 485 the 2023 ice extent to that in 2012.

486 Following the same steps as in Secs. V A and V C, the IM sim-
 487 ulations are conducted for the period of June 16 2012 to January 1
 488 2013 for the focus area. To keep the paper concise, we will skip the
 489 semi-monthly actual and simulated images and the best-fit param-
 490 eters, which will be provided by the author upon reasonable request.
 491 The more informative ice coverage and extent comparison charts
 492 are nevertheless included in Fig. 14.

493 Comparing Fig. 13 with Fig. 14 indicates that 2023 did not
 494 break the record-low Arctic sea ice extent level set in 2012, vali-
 495 dated by both the actual measures and the IM simulations.
 496 However, 2023 sets the second lowest ice extent for our focus area,
 497 below those low levels previously achieved in 2019 and 2020 [for
 498 the entire Arctic region not limited to our focus area, 2023 marks
 499 the 6th-lowest ice extent in history;⁴⁷ all six minimums are well
 500 within small margins]. (2019 and 2020 results are not included in
 501 this paper but can be provided upon request). Even though 2023
 502 does not break the historical record, it offers no reason for us to be
 503 optimistic about the future. In fact, in the 45-year-satellite record
 504 from 1979 to 2023, 17 of the lowest minimums have all occurred in
 505 the last 17 years.⁴⁷ Many scientists are concerned that the effect of
 506 Arctic sea ice decline on global warming will intensify as the sea ice
 507 loss continues.^{48,49} Although predicting the ice extent for the future
 508 years is beyond the scope of our current study, we will discuss the
 509 possibilities in Sec. VI.

510 VI. DISCUSSION AND FUTURE WORK

511 In this paper, we introduce continuous spin values and an
 512 inertia factor to a classical 2D IM and utilize this generalized
 513 model simulate the dynamics of the sea ice evolution in the Arctic
 514 region by employing the Metropolis-Hastings algorithm. Our
 515 results show excellent similarity with the actual sea ice dynamics,
 516 based on the ice configurations and the numerical measures includ-
 517 ing the ice coverage percentage and the ice extent, and, therefore,
 518 unleash the potential of the 100-year-old classical Ising model in
 519 climate change research and other interdisciplinary science studies.

520 A. Discussions on the methodology

521 The extrapolation ability of our generalized model is worth
 522 discussing. In other words, how does the model perform if the
 523 Ising parameters fitted from one year are applied to the data of
 524 another year? For this purpose, we conduct projection of sea ice
 525 evolution from September to December 2023 based on the 2022
 526 best-fit parameters in Table I for the same time periods with the
 527 initial ice image on August 16 2023. Our projection displays larger
 528 discrepancies from the actual images compared to Fig. 12, since the
 529 idiosyncratic intra-year configurations are hard to be reproduced by
 530 the Ising parameters from a different year. However, even though
 531 the extrapolation ability of the Ising parameters is far from being
 532 perfect, the ice extent metrics calculated from our experiment

533 accurately predicts that September 2023 would record the second
 534 lowest ice extent in history for our focus area.

535 The impact of the inertia factor I on the performance of our
 536 model is also worth discussing. In fact, we have explored the
 537 vanilla Ising model without the inertia term; the subsequent
 538 simulation results substantially underperform the results with
 539 the inertia term incorporated. This finding validates the signifi-
 540 cant strength of the inertia factor in sea ice modeling, indicating
 541 that Arctic sea ice and water indeed display the tendency to stay
 542 unchanged. However, our finding does not confirm that the
 543 inertia factor is a must-have; it is possible to improve the Ising
 544 model performance via other routes, e.g., by further enriching
 545 the functional forms of the external force B , which is out of
 546 scope of this paper.

547 Details of the above analyses are not included to keep our
 548 paper concise. They can be shared by the author upon reasonable
 549 request.

550 B. Will a “Blue Ocean Event” happen? If so, when will it
 551 be?

552 Arctic sea ice extent in September 2023 was near the historic
 553 minimum achieved in 2012. As the Arctic sea ice continues to shrink,
 554 will a “Blue Ocean Event” take place, i.e., will we see an “ice-free”
 555 Arctic Ocean? Some research predicts that it can happen in the 2030s.⁴⁸

556 Our current study will need to be extended to gain the full pre-
 557 dictive power when utilized to answer this “Blue Ocean Event” ques-
 558 tion. As shown in Tables I and II, the best-fit IM parameters
 559 demonstrate the substantial impact of the external force factor B ,
 560 which remains unexplored within the scope of our model. If the func-
 561 tional form of this external force is further enriched and linked to the
 562 actual environmental factors in climate change modeling, the IM
 563 framework may prove its strength in offering the “Ising Prediction” to
 564 answer the “Blue Ocean Event” question.

565 C. Quantum Ising model

566 Our study sets the stage for future Ising model research on sea
 567 ice evolution. Methodologically, besides the continuous spin IM, a
 568 much more complicated alternative idea to be explored in future
 569 research is the quantum Ising model (QIM), or the so-called trans-
 570 verse field Ising model,^{50,51} by which the continuous spin values can
 571 be modeled by the rotation of qubits in the Bloch Sphere.⁵² Once
 572 quantum computers are accessible for personal usage,⁵³ our research
 573 can be readily extended with the assistance of quantum computing
 574 in the future.

575 ACKNOWLEDGMENTS

576 We thank the National Snow and Ice Data Center (NSIDC)
 577 and the National Aeronautics and Space Administration (NASA)
 578 for generously making the data publicly available and providing
 579 data support for this research. We also thank Professor Joan Wang
 580 at the Xiamen University Malaysia Department of Physics and Dr.
 581 Alyssa Shearer at Horace Mann School for their valuable guidance
 582 and support for this research.

583 **AUTHOR DECLARATIONS**584 **Conflict of Interest**

585 The author has no conflicts to disclose.

586 **Author Contributions**

587 **Ellen Wang:** Conceptualization (equal); Data curation (equal);
 588 Formal analysis (equal); Investigation (equal); Methodology
 589 (equal); Project administration (equal); Software (equal);
 590 Validation (equal); Visualization (equal); Writing – original draft
 591 (equal); Writing – review & editing (equal).

592 **DATA AVAILABILITY**

593 The Near-Real-Time DMSP SSMIS Daily Polar Gridded Sea
 594 Ice Concentrations' (NRTSI) data used in this study are publicly
 595 available on National Snow and Ice Data Center (NSIDC) website
 596 <https://nsidc.org/data/nsidc-0081/versions/2>. The data that support
 597 the findings of this study are available from the corresponding
 598 author upon reasonable request.

599 **REFERENCES**

- Q5 600 ¹NSIDC, "Arctic sea ice news and analysis" (2021).
 Q6 601 ²NASA, "Arctic sea ice minimum extent" (2022).
 Q7 602 ³NOAA National Centers for Environmental Information, see [https://www.climate.gov/news-features/featured-images/2023-was-warmest-year-modern-temperature-record#:~:text=The%20year%20was%20the,decade%20\(2014%E2%80%932023\)](https://www.climate.gov/news-features/featured-images/2023-was-warmest-year-modern-temperature-record#:~:text=The%20year%20was%20the,decade%20(2014%E2%80%932023)) for "Climate.gov" (January 2024).
 Q8 603 ⁴E. Ising, "Beitrag zur Theorie des Ferromagnetismus," *Z. Phys.* **31**(1), 253–258 (1925).
 604 ⁵E. Ising, "Contribution to the theory of ferromagnetism," *J. Math. Phys.* **12**, 226 (1924).
 605 ⁶G. S. Sylvester and H. van Beijeren, "Phase transitions for continuous-spin Ising ferromagnets," *J. Funct. Anal.* **28**, 145–167 (1978).
 606 ⁷E. Bayong and H. T. Diep, "Effect of long-range interactions on the critical behavior of the continuous Ising model," *Phys. Rev. B* **59**(18), 883 (1999).
 607 ⁸N. Metropolis, A. W. Rosenbluth, M. N. Rosenbluth, A. H. Teller, and E. Teller, "Equation of state calculations by fast computing machines," *J. Chem. Phys.* **21**(6), 1087 (1953).
 608 ⁹W. Meiser, J. Steward, H. Wilcox, M. Hardman, and D. Scott, "Near-real-time DMSP SSMIS daily polar gridded sea ice concentrations, version 2," in *NASA National Snow and Ice Data Center Distributed Active Archive Center*, Boulder, Colorado (■, 2023).
 609 ¹⁰S. G. Brush, "History of the Lenz-Ising model," *Rev. Mod. Phys.* **39**(4), 883 (1967).
 610 ¹¹L. Onsager, "Crystal statistics. I. A two-dimensional model with an order-disorder transition," *Phys. Rev.* **65**(3–4), 117–149 (1944).
 611 ¹²H. A. Kramers and G. H. Wannier, "Statistics of the two-dimensional ferromagnet: Part I," *Phys. Rev.* **60**(3), 252–262 (1941).
 612 ¹³H. A. Kramers and G. H. Wannier, "Statistics of the two-dimensional ferromagnet: Part II," *Phys. Rev.* **60**(3), 263–276 (1941).
 613 ¹⁴J. Zuber and C. Itzykson, "Quantum field theory and the two-dimensional Ising model," *Phys. Rev. D* **15**, 2875 (1977).
 614 ¹⁵M. Aguilera, S. A. Moosavi, and H. Shimazaki, "A unifying framework for mean-field theories," *Nat. Commun.* **12**, 1197 (2021).
 615 ¹⁶S. Sides, P. Rikvold, and M. Novotny, "Kinetic Ising model in an oscillating field: Finite-size scaling at the dynamic phase transition," *Phys. Rev. Lett.* **81**(4), 4865 (1998).
 616 ¹⁷D. Stauffer, "Social applications of two-dimensional Ising models," *Am. J. Phys.* **76**(4), 470–473 (2008).
 617 ¹⁸C. Campajola, F. Lillo, and D. Tantari, "Inference of the kinetic Ising model with heterogeneous missing data," *Phys. Rev. E* **99**(6), 062138 (2019).
 618 ¹⁹B. Dunn and Y. Roudi, "Learning and inference in a nonequilibrium Ising model with hidden nodes," *Phys. Rev. E* **87**(2), 022127 (2013).
 619 ²⁰N. N. Vtyurina, D. Dulin, M. W. Docter, A. S. Meyer, N. H. Dekker, and E. A. Abbondanzieri, "Hysteresis in DNA compaction by Dps is described by an Ising model," *Proc. Natl. Acad. Sci. U.S.A.* **113**(18), 4982–4987 (2016).
 620 ²¹J. Majewski, H. Li, and J. Ott, "The Ising model in physics and statistical genetics," *Am. J. Hum. Genet.* **69**(4), 853–862 (2001).
 621 ²²A. Witoelar and Y. Roudi, "Neural network reconstruction using kinetic Ising models with memory," *BMC Neurosci.* **12**, 274 (2011).
 622 ²³C. Donner and M. Opper, "Inverse Ising problem in continuous time: A latent variable approach," *Phys. Rev. E* **96**, 061104 (2017).
 623 ²⁴J. Hertz, Y. Roudi, and J. Tyrcha, "Ising model for inferring network structure from spike data," *arXiv.1106.1752* (2011).
 624 ²⁵Y. Roudi, B. Dunn, and J. Hertz, "Multi-neuronal activity and functional connectivity in cell assemblies," *Curr. Opin. Neurobiol.* **32**, 38 (2015).
 625 ²⁶Y. Shi and T. Duke, "Cooperative model of bacteril sensing," *Phys. Rev. E* **58**(5), 6399–6406 (1998).
 626 ²⁷T. F. Stepinski, "Spatially explicit simulation of deforestation using the Ising-like neutral model," *Environ. Res.* **2**(2), 025003 (2023).
 627 ²⁸T. F. Stepinski and J. Nowosad, "The kinetic Ising model encapsulates essential dynamics of land pattern change," *R. Soc. Open Sci.* **10**(10), 231005 (2023).
 628 ²⁹Y.-P. Ma, I. Sudakov, C. Strong, and K. Golden, "Ising model for melt ponds on Arctic sea ice," *New J. Phys.* **21**, 063029 (2019).
 629 ³⁰T. C. Schelling, "Dynamic models of segregation," *J. Math. Sociol.* **1**, 143–186 (1971).
 630 ³¹J. P. Bouchaud, "Crises and collective socio-economic phenomena: Simple models and challenges," *J. Stat. Phys.* **151**, 567–606 (2013).
 631 ³²S. Bornholdt and F. Wagner, "Stability of money: Phase transitions in an Ising economy," *Physica A* **316**(1–4), 453–468 (2002).
 632 ³³United States Environmental Protection Agency, see <https://www.epa.gov/climate-indicators/climate-change-indicators-arctic-sea-ice#:~:text=September%20is%20typically%20when%20the,maximum%20extent%20after%20winter%20freezing> "Climate Change Indicators: Arctic Sea Ice" (2021).
 633 ³⁴R. Lindsey and M. Scott, "Climate change: Arctic sea ice summer minimum," Climate.gov (2022).
 634 ³⁵NASA Langley Research Center's Atmospheric Science Data Center, *Ice-Albedo Feedback in the Arctic* (NASA, 2020).
 635 ³⁶K. L. Oakley, M. E. Whalen, D. C. Douglas, M. S. Udevitz, T. C. Atwood, and C. Jay, *Polar Bear and Walrus Response to the Rapid Decline in Arctic Sea Ice* (USGS—Science for a changing world, 2012), see <https://pubs.usgs.gov/publication/f20123131>.
 636 ³⁷NSIDC, "EASE-Grid Sea Ice Age, Version 4" (2021).
 637 ³⁸World Meteorological Organization, "Copernicus confirms July 2023 was the hottest month ever recorded" (2023).
 638 ³⁹Copernicus, see [https://climate.copernicus.eu/record-warm-november-consolidates-2023-warmest-year#:~:text=The%20extraordinary%20global%20November%20temperatures,Climate%20Change%20Service%20\(C3S\)](https://climate.copernicus.eu/record-warm-november-consolidates-2023-warmest-year#:~:text=The%20extraordinary%20global%20November%20temperatures,Climate%20Change%20Service%20(C3S)) for "Record Warm November Consolidates 2023 as the Warmest Year" (2023).
 639 ⁴⁰L. Boltzmann, "Studies on the balance of living force between moving material points," *Wiener Berichte* **58**, 517–560 (1868).
 640 ⁴¹A. Shekaari and M. Jafari, "Theory and simulation of the Ising model," *arXiv* (2021).
 641 ⁴²M. Krasnytska, B. Berche, Y. Holovatch, and R. Kenna, "Ising model with variable spin/agent strengths," *J. Phys. Complex* **1**, 035008 (2020).
 642 ⁴³Y. Hu, R. M. Horton, M. Song, and J. Liu, "Reducing spread in climate model projections of a September ice-free Arctic," *Proc. Natl. Acad. Sci. U.S.A.* **110**(31), 12571–12576 (2013).
 643 ⁴⁴G. J. Roy, "Time-dependent statistics of the Ising model," *J. Math. Phys.* **4**(2), 294–307 (1963).
 Q9

- 701 ⁴⁵C. Tsallis and D. Stariolo, "Generalized simulated annealing," *Physica A* **233**,
702 395–406 (1996).
703 ⁴⁶Y. Xiang, D. Sun, W. Fan, and X. Gong, "Generalized simulated annealing
704 algorithm and its application to the Thomson model," *Phys. Lett. A* **233**,
705 216–220 (1997).
706 ⁴⁷See <https://nsidc.org/arcticseaincnews/2023/09/arctic-sea-ice-minimum-at-sixth/>
707 for "Arctic sea ice minimum at sixth lowest extent on record," National Snow & Ice
708 Data Center (2023).
709 ⁴⁸Y.-H. Kim, S.-K. Min, N. P. Gillett, D. Notz, and E. Malinina,
710 "Observationally-constrained projections of an ice-free Arctic even under a low
711 emission scenario," *Nat. Commun.* **14**, 3139 (2023).
712
713
714
715
716
717
718
719
720
721
722